DOI: 10.26599/FSHW.2025.9250508

Contents lists available at SciOpen

Food Science and Human Wellness

journal homepage: https://www.sciopen.com/journal/2097-0765

China Food Publishing Co.

The Extract of *Polygonum capitatum* Alleviates Hyperoxaluria-Induced Oxidative Stress by Targeting the PI3K-ERK-NRF2 Signaling Pathway.

Kai Li[a,c], Songsong Tan[a], Hao Su[a], Lin Wei[a], Weiming Chen[c], Dongbo Yuan[a], Bo Yan[a], Fa Sun[a], Can Li[b,*], Kehua Jiang[a,*], Jianguo Zhu[a,b,c*].

[a] *Department of Urology, Guizhou Provincial People's Hospital, The Affiliated Hospital of Guizhou University, Guiyang, Guizhou Province, 550002, China*

[b] *Provincial Key Laboratory for Rare Animal and Economic Insect of the Mountainous Region, College of Biology and Environmental Engineering, Guiyang University, Guiyang, 550025, China*

[c] *Medical College of Guizhou University, Guiyang, Guizhou Province, 550002, China*

ABSTRACT: *Persicaria capitata* (Buch.-Ham. ex D. Don) H. Gross is a perennial herb belonging to the Polygonaceae family, mainly distributed in southwestern China. *Persicaria capitata* is edible and boasts a high nutritional profile, and the entire plant serves medicinal purposes. According to the *Guangxi Materia Medica*, it has the functions of "relieving wind-dampness, enhancing blood circulation, and easing pain". *Persicaria capitata* is a major component of the traditional Chinese medicine formula, Re-Lin-Qing, which is widely used for treating urinary calculi (urolithiasis). However, its specific mechanisms of action remain unclear. In this study, we employed molecular biology, molecular dynamics, and cellular biology strategies to develop a rat experimental model of oxalate-induced urolithiasis and a cell model of oxalate-induced injury to study the active constituents and molecular mechanisms of *Persicaria capitata* in inhibiting oxalate stone formation both in vivo and in vitro. The results show that in vivo, *Persicaria capitata* significantly reduced the formation rate of oxalate stones in rats, decreased the levels of urinary oxalate, sodium, potassium, calcium, and magnesium, while increasing urine pH, urinary citrate levels, and urine excretion. Moreover, *Persicaria capitata* significantly lowered serum creatinine levels in oxalate stone model rats and mitigated kidney damage. In vitro, treatment with *Persicaria capitata* extract effectively alleviated oxalate-induced oxidative stress in HK-2 cells, reducing the levels of reactive oxygen species (ROS) and malondialdehyde (MDA), while increasing ATP levels and inhibiting oxalate-induced apoptosis. LC-MS analysis of *Persicaria capitata* components, in combination with transcriptomics, network pharmacology, and metabolomics sequencing, indicated that Myricetin might be one of its potential bioactive compounds. Both *Persicaria capitata* extract and its active compound, Myricetin, significantly reversed the oxalate-induced decrease in PI3K and ERK levels and inhibited the overexpression of oxidative stress-related proteins. Further analysis using cellular thermal shift assay (CETSA) and drug affinity responsive target stability (DARTS) experiments revealed that Myricetin exhibits strong binding affinity to PIK3CA. Moreover, PI3K inhibitors reversed the protective effects of *Persicaria capitata* and Myricetin on oxalate-induced cell injury models. *Persicaria capitata* exerts its anti-urolithiasis effects by alleviating oxidative stress through a multi-component, multi-target synergistic mechanism. Additionally, Myricetin, one of the bioactive components of *Persicaria capitata*, directly binds to

***Corresponding author**
lican790108@163.com (C. Li); 4158273@qq.com(K.Jiang); Doctorzhujianguo@163.com (J. Zhu).

Received 18 October 2024
Received in revised from 17 December 2024
Accepted 2 January 2025

PIK3CA, promoting ERK expression, upregulating NRF2 levels, and subsequently reducing oxidative stress, thereby inhibiting oxalate stone formation and alleviating kidney injury.

Keywords: kidney stones, *Persicaria capitata*, oxidative stress, Myricetin, PIK3CA.

1. Introduction

Kidney stones are a common disease with increasing incidence and recurrence rates, posing a growing global health threat[1-2]. The occurrence of kidney stones surpasses 14.8%, and the recurrence rate can reach up to 50% within five years[3]. Calcium oxalate stones account for over 80% of cases, and elevated oxalate levels may lead to chronic kidney disease (CKD)[4-5].

Oxidative stress-induced renal epithelial cell injury is a key pathological factor in the formation of oxalate stones. The excessive buildup of reactive oxygen species (ROS) results in oxidative stress. a hallmark of renal injury, which further results in mitochondrial dysfunction and apoptosis of renal tubular epithelial cells[6-10]. Reactive oxygen species (ROS) are inherent by-products of mitochondrial respiration, which are usually cleared by the antioxidant system. When ROS levels surpass the antioxidant capacity of the cell, it can lead to cellular damage. The cellular antioxidant system can quickly convert ROS into less reactive or non-reactive forms, utilizing the glutathione and thioredoxin redox cycles, as well as antioxidant enzymes such as superoxide dismutase (SOD), catalase, and glutathione peroxidase (Gpx). In most idiopathic stone formers, excessive oxidative stress heightens the risk of crystals adhering to renal epithelial cells. Fragments of damaged cells can facilitate crystal nucleation, facilitating the aggregation of crystals into kidney stones. Additionally, oxidative stress is a major driver of other kidney diseases[11]. Oxalate-induced renal epithelial cell injury increases the expression of adhesion proteins, particularly osteopontin (OPN), CD44, and inflammatory factors IL-6 and MCP-1, thereby elevating inflammation and adhesion risks, which further promote the formation of stone crystals. Therefore, reducing oxalate levels, protecting cells from oxidative damage, and inhibiting oxidative stress are effective strategies for treating kidney stones[12-13].

Oxidative stress primarily involves signaling pathways like PI3K/AKT, NRF2, and NF-kappaB[14-16]. Among these, the PI3K is particularly closely related to oxidative stress. The phosphoinositide 3-kinase (PI3K) pathway is an intracellular signaling pathway associated with cell growth, proliferation, and survival[17]. ROS can both regulate the PI3K pathway to induce mitochondrial damage and promote apoptosis through this pathway[18-19]. On one hand, the PI3K signaling pathway can trigger mitochondrial damage, increasing oxidative stress levels and creating a microenvironment that facilitates crystal adhesion. On the other hand, the PI3K pathway exacerbates oxidative stress levels by promoting apoptosis[20-21].

Persicaria capitata (Buch.-Ham. ex D. Don) H. Gross is a perennial herb belonging to Polygonaceae family, mainly distributed in southwestern China. *Persicaria capitata* is edible and boasts a high nutritional profile, including vitamins, an abundance of essential minerals, and various other nutrients. It contains at least 17 amino acids, 7 of which are essential for human health. Its seeds can be processed to extract oil and also serve as a good nectar source for bees. When cooked with other ingredients, it enhances the flavor and nutritional value of soups. it is known for its alcohol-detoxifying properties, which is why it was traditionally

used by ancient people as an accompaniment to alcohol consumption. Additionally, the whole plant of *Persicaria capitata* is used medicinally[22]. According to the *Guangxi Materia Medica*, it has the functions of "alleviating wind-dampness, improving blood circulation, and reducing pain"[23]. *Persicaria capitata* is a major component of the traditional Chinese medicine formula Re-Lin-Qing Granules, and although it is widely used in clinical treatment of stones[24-25], its specific mechanisms of action remain unclear. In this study, we utilized molecular biology, molecular dynamics, and cellular biology approaches to establish an oxalate stone rat model and a hyperoxaluria-induced cell injury model to examine the bioactive constituents and the molecular mechanisms of *Persicaria capitata* in inhibiting oxalate stone formation both in vivo and in vitro, with the aim of providing theoretical support for its clinical application.

2. Materials and Methods

2.1 Reagents

Reactive Oxygen Species (ROS) assay kit (Solarbio, Shanghai, CA1410); CCK-8 kit (MCE, Shanghai, HY-K0301); MDA kit (Solarbio, Shanghai, BC0025); ATP assay kit (Solarbio, Shanghai, BC0300); SOD kit (Solarbio, Shanghai, BC0170); Apoptosis detectionkit (KeyGENBioTECH, Nangjin, Jiangshu, KGA108-1); LY29400(purity ≥ 99%) (MCE, Shanghai, HY-101108); ML385(purity ≥ 99%) (MCE, Shanghai, HY-123693). The *Persicaria capitata* were provided by Weimen Pharmaceutical Co., Ltd. (Guizhou), batch number: 21062D. The stone-expelling granules (National Drug Approval Number Z32020071).

2.2. Animal model of kidney stones

A total of 72 healthy male rats, (6-7)weeks old, weighing (225 ± 30) g, were obtained through Chongqing Laboratory Animal Research Center (Animal license: SCXK(Chongqing)2021-0010). The rats were housed under controlled conditions ((21-24) ℃; humidity: (50 ± 10)%; free access to food and water). After one week divided into six groups (n=12 per group):

- Group A (Control): Normal diet without any interventions.
- Group B (Model): Oxalate-induced stone formation without drug treatment.
- Group C: Treated with stone-expelling (PSKL) granules.
- Group D: Low dose of *Persicaria capitata*.
- Group E: Medium dose of *Persicaria capitata*.
- Group F: High dose of *Persicaria capitata*.

During the modeling period, rats were fed a diet containing 1.2% ethylene glycol for one week to induce stone formation.

2.3 Treatment with Persicaria capitata and measurement of biological indicators

The aqueous extract (powder) of *Persicaria capitata* was provided by Weimen Pharmaceutical Co., Ltd. (Guizhou). The dosage was calculated based on a 60 kg adult human equivalent and adjusted according to the body weight of the rats (200 g). The aqueous extract (powder) of *Persicaria capitata* was dissolved in PBS and administered by gavage with a volume of 4 mL. the control group and the model group were gavaged

with the same volume of PBS, the drug concentration of each drug group is as follows according to the weight of rats:

- The Stone-expelling granules group: 2.7 g/kg Stone-expelling granules.
- The Low dose of *Persicaria capitata* group: 2.16 g/kg *Persicaria capitata*.
- The Medium dose *Persicaria capitata* group: 4.32 g/kg *Persicaria capitata*.
- The High dose *Persicaria capitata* group: 8.64 g/kg *Persicaria capitata*.

On the day before tissue collection, 24 hour urine was collected from each rat using metabolic cages. The urine volume was measured, and supernatants were sent for analysis of oxalate concentration using ion chromatography. Other electrolyte levels (K^+, Ca^{2+}, Na^+, Mg^{2+}) were measured using an automatic biochemical analyzer. Blood samples were also collected from the abdominal aorta for further analysis of serum creatinine and electrolyte concentrations. Kidneys were fixed in 10% formalin and subjected to histopathological examination, including HE staining and paraffin embedding for microscopic analysis of crystal formation and tissue damage. Crystal grades were assessed as follows:

- 0: No crystals observed.
- I: Small, sparse crystals.
- II: Clusters of large crystals.
- III: Aggregates of crystals linked together.
- IV: Large, sheet-like crystal formations.

2.4 Cell culture

HK-2 and NRK kidney epithelial cells were purchased from Wuhan Puno Biotechnology Co., Ltd. Cells were cultured in DMEM containing 10% fetal bovine serum (FBS) and 1% penicillin-streptomycin. Cultures were maintained at 37 ℃ in a 5% CO_2 incubator.

2.5 Transcriptome sequencing

Kidney tissue samples were ground into a fine powder and RNA was extracted. Total RNA was purified and quality-controlled for transcriptome sequencing using the Illumina PE150 platform. Differential expression was determined with log2 (Fold Change) > 0.5 and padj < 0.05. Further analyses, such as KEGG and GO pathway enrichment, were performed.

2.6 Analysis of Persicaria capitata components

The components of *Persicaria capitata* were analyzed using Vanquish UHPLC and Q Exactive Focus mass spectrometry (Thermo Fisher Scientific). The sample preparation involved extracting 100 mg of the herb with a methanol-water mixture (4:1), followed by vortexing, homogenizing, ultrasonication, and filtration. Chromatographic separation was achieved on a Waters UPLC BEH C_{18} column.

2.7 Network pharmacology

Targets of the ingredients of *Persicaria capitata* were obtained using the SwissTarget database (https://swisstargetprediction.ch/). The GeneCard database (https://www.genecards.org/), OMIM database

(https://www.omim.org/), and TTD database (https://db.idrblab.net/ttd/) were utilized to acquire targets related to "kidney stones". The Metascape database (https://metascape.org/) was employed to analyze the KEGG and GO signaling pathways of the common targets between *Persicaria capitata*-kidney stones. The STING database (https://cn.string-db.org/) was used to construct a PPI network for the common targets of *Persicaria capitata* and kidney stones, and the "cytoNAC" plugin in Cytoscape 3.5.1 was used to analyze the top 10 targets among the common targets, identified as core targets. The PubChem database (https://pubchem.ncbi.nlm.nih.gov/) was utilized to obtain the 3D structures of the components of *Persicaria capitata*, while the RCSB PDB website (https://www.rcsb.org/) provided the 3D structures of the proteins. Molecular docking was performed using AutoDock Vina.

2.8 Molecular dynamics simulation

Molecular dynamics simulations were conducted using Gromacs 2022.3. Small molecules were parameterized using AmberTools22, and RESP charges were calculated. Simulations were conducted under NVT and NPT conditions at 300 K, with a total run time of 100 ns. Analyses included calculating RMSD, RMSF, radius of gyration, and free energy landscape.

2.9 Metabolomics

This study investigated the metabolic differences between samples using a UPLC-MS/MS detection platform, a self-constructed database, and multivariate statistical analysis. Rat kidney tissues were collected, and the lysate was extracted. After LC-MS analysis, the raw data were obtained and subjected to processing, quality control, and bioinformatics analysis, followed by an analysis of the differential metabolites.

2.10 ROS detection

Prior to detection, tissue or adherent cells were digested into a cell suspension. DCFH-DA was diluted in serum-free culture medium at a ratio of 1:1000 to achieve a final concentration of 10 μmol/L. After collection, the cells were suspended in the diluted DCFH-DA solution at a concentration of 1×10^6 cells/mL and incubated in a 37 ℃ cell incubator for 20 minutes. The mixture was inverted and gently mixed every 3-5 minutes to ensure sufficient contact between the probe and the cells. The cells were washed three times with serum-free cell culture medium to thoroughly eliminate any unincorporated DCFH-DA. Detection was carried out using an excitation wavelength of 488 nm and an emission wavelength of 525 nm.

2.11 SOD detection

Adherent cells were washed with pre-cooled PBS or saline at 4 ℃ or in an ice bath. A volume of 100 μL of SOD sample preparation solution was added for every 1×10^6 cells, and the cells were gently pipetted to ensure complete lysis. An appropriate amount of WST-8/enzyme working solution was prepared for a total reaction volume of 160 μL. The WST-8/enzyme working solution and activation working solution were mixed in a volume of 160 μL. A 96-well plate was set up with sample wells and various blank control wells. The mixture was incubated at 37 ℃ for 30 minutes. The absorbance was measured at 450 nm.

2.12 ATP content detection

A total of 1×10^6 cells were resuspended in 1 mL of extraction buffer and subjected to ultrasonic disruption (ice bath, power 200 W, ultrasonic for 2 s, pause for 1 s, total time 1 min), followed by centrifugation at 10,000 g at 4 ℃ for 10 minutes. Then, 100 μL of a 10 μmol/L ATP standard solution was mixed with 1.5 mL of distilled water to prepare a 0.625 μmol/L standard solution, which was used after preheating at 37 ℃ for 10 minutes. Sample measurements were performed according to the required reagent ratios.

2.13 MDA detection

Cells were collected and centrifuged to remove the supernatant, following the addition of 1 mL of extraction buffer, the cells were lysed using ultrasonic disruption and then centrifuged at 8000 g at 4 ℃ for 10 minutes. The supernatant was collected, and the mixture was incubated in a water bath at 100 ℃ for 60 minutes, then cooled in an ice bath and centrifuged at 10,000 g at room temperature for another 10 minutes. A 200 μL aliquot of the supernatant was placed into a microglass cuvette or a 96-well plate, and the absorbance of each sample was measured at 532 nm and 600 nm.

2.14 Cell viability assay

Cell viability was assessed using the CCK8 assay. A total of 4×10^3 cells were seeded into 96-well plates and cultured for 24 hours. The cells were then treated with different drugs and further cultured for 48 hours. Afterward, 10 μL of CCK8 reagent was added to each well, followed by incubation at 37 ℃ in the dark for 1.5 hours. The absorbance was measured at 450 nm using a microplate reader.

2.15 TUNEL staining

Kidney tissues were dewaxed in xylene for 5-10 minutes and then treated with 20 μg/mL of DNase-free proteinase K at (20-37) ℃ for (15-30) minutes. The samples were washed three times with PBS or HBSS. They were then incubated at room temperature for 20 minutes in 3% hydrogen peroxide solution (3% H_2O_2 in PBS) to inactivate endogenous peroxidases in the sections. After that, the samples were washed three times with PBS or HBSS. Following one wash with PBS or HBSS, 0.1-0.3 mL of the labeling reaction stop solution was added, and the samples were incubated at room temperature for 10 minutes. Finally, the samples were washed three times with PBS or HBSS, and DAB chromogen solution was used for coloration.

2.16 Cell apoptosis assay

Cells were digested with trypsin without EDTA, and the digestion was stopped using complete medium. The cells were collected into centrifuge tubes, balanced, and then centrifuged at 1200 r/min for 5 minutes. The supernatant was discarded, and the cell pellet was retained. Pre-cooled 1× bending buffer (100 μL) was added to the cell pellet, and the cells were gently resuspended by pipetting. Each sample was stained with 5 μL of FITC and 5 μL of PI dye, and incubated for 15 minutes in the dark. After staining, 400 μL of cold 1× bending buffer was added to every sample, gently mixed, and the samples were evaluated with a flow cytometer.

2.17 Transmission electron microscopy (TEM)

Images were obtained using a JEM-1400FLASH transmission electron microscope (JEOL, Japan). The entire tissue was initially examined at low magnification, and images of specific areas with lesions were captured. The samples were pre-fixed (customer fixation) and then fixed with 1% osmium tetroxide.

Sequential dehydration was performed using acetone, followed by infiltration with a dehydration agent and Epon-812 embedding agent. The samples were embedded in pure Epon-812, Ultrathin sections measuring 60-90 nm were prepared using an ultramicrotome and placed on copper grids. The sections were stained with uranyl acetate for (10-15) minutes, followed by lead citrate staining for (1-2) minutes at room temperature.

2.18 Immunohistochemistry

After the tissue was fixed with paraformaldehyde, embedded, sectioned, and mounted, deparaffinization and hydration were performed using xylene. Antigen retrieval was carried out with a retrieval solution, subsequently followed by two washes with PBS, each lasting 5 minutes. After blocking non-specific binding sites, the tissue was washed, counterstained with hematoxylin, dehydrated, and imaged under a microscope for documentation.

2.19 CETSA

Total cellular proteins were extracted and divided into the treatment group and the control group. The treatment group was treated with the Myricetin (200 μM), while the control group received the same concentration of DMSO. The proteins were heated using a metal bath for 5 minutes at sequential temperatures of 37 ℃, 40 ℃, 43 ℃, 46 ℃, 49 ℃, 52 ℃, 55 ℃, and 58 ℃. Protein immunoblotting was subsequently performed to detect the binding between the target protein and small molecules.

2.20 DARTS

Similar to the CETSA experiment to obtain proteins. Different concentrations of Pronase, ranging from 1:0, 1:250, 1:500, and 1:1000, were added to both groups. The treatment group was treated with 200 μM of the drug, while the control group was given the same concentration of DMSO. The samples were adjusted to 40 ℃ (the optimal temperature for enzyme activity) for 30 minutes and subjected to protein denaturation. Protein immunoblotting was then performed for analysis.

2.21 Western blot

The pre-cooled RIPA lysis buffer was used to lyse the total cellular proteins (12,000 r/min, 10 min). And 1/4 volume of loading buffer was added. After mixing, the sample was heated at 100 ℃ for 10 minutes. 40 μg protein was separated by SDS-PAGE and then transferred to a PVDF membrane. PI3 Kinase p110 Alpha antibody (proteintech, 67071-1-Ig), ERK1/2 antibody (proteintech, 66192-1-Ig), NRF2 antibody (proteintech, 16396-1-AP), HO-1/HMOX1 antibody (proteintech, 10701-1-AP), SOD antibody (proteintech, 10269-1-AP), Osteopontin antibody (proteintech, 22952-1-AP), NOX4antibody (proteintech, 14347-1-AP), NOX2 antibody (proteintech, 19013-1-AP). GAPDH antibody (proteintech, 10494-1-AP). The membrane □□s Subsequently incubated with primary and secondary antibodies, followed by exposure. Finally, ImageJ software was used to analyze the grayscale values of the proteins.

2.22 Statistical analysis

All experiments were repeated independently no less than 3 times. Show one of the three experimental results in the picture. Data were expressed as mean ± SD and analyzed using SPSS26.0 and GraphPad Prism 9.0 software. Statistical comparisons were performed using ANOVA or t-tests, with significance levels of $^{**}P < 0.01$,$^{*}P < 0.05$.

3. Results

3.1 Persicaria capitata reduces oxalate stone formation in vivo

To evaluate the therapeutic potential of *Persicaria capitata* against oxalate stones in vivo, we established a rat model of oxalate stones. After the treatment, HE staining of kidney sections revealed the following: in the control group, the renal medulla and cortex remained intact with no evident calcium oxalate crystals (Fig. 1A). In the model group, extensive grade IV calcium oxalate crystal aggregation and severe epithelial inflammation were observed (Fig. 1B). In both the PSKL group and the medium-dose *Persicaria capitata* group, only minor tissue damage was detected, though the PSKL group showed a more pronounced punctate distribution of calcium oxalate crystals compared to the medium-dose *Persicaria capitata* group (Fig. 1C and 1E). In terms of efficacy evaluation, the degree of stone formation in rats was ranked as follows: model group (100.0%) > high-dose *Persicaria capitata* group (75.0%) > low-dose *Persicaria capitata* group (70.8%) > PSKL group (62.5%) > medium-dose *Persicaria capitata* group (58.3%) > control group (0.0%) (Fig. 1G). Compared to the model group, stone formation was significantly reduced following treatment with *Persicaria capitata.* All treatment groups, including low-, medium-, and high-dose *Persicaria capitata* and the PSKL, were effective in reducing kidney calcium oxalate stones, with the medium-dose *Persicaria capitata* group demonstrating the best effect, followed by the PSKL group and the low-dose *Persicaria capitata* group, with the high-dose *Persicaria capitata* group showing the least effect.

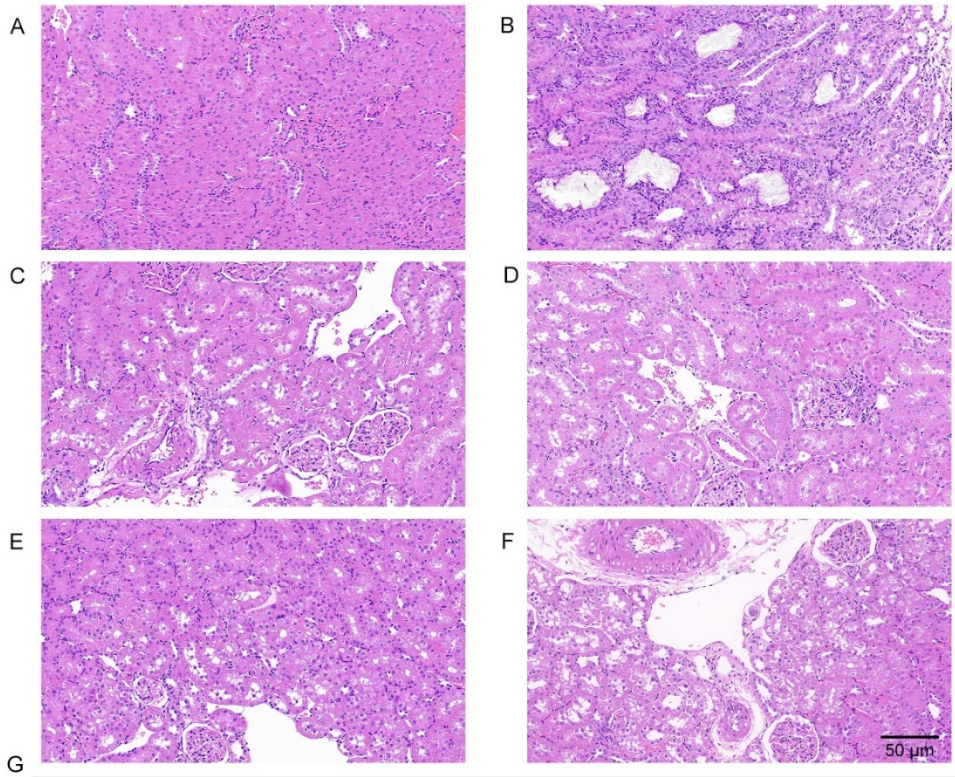

G

Group	0	I	II	III	IV	Total	Lithogenesis rate (%)	Crystallization are (%)
A	24	0	0	0	0	24	0.0%	0.00
B	0	3	8	10	3	0	100.0%*	4.38±2.08*
C	15	6	2	1	0	15	62.5%*#	2.01±1.15#*
D	17	5	2	0	0	17	70.8%*#	2.54±1.07#*
E	14	7	3	0	0	14	58.3%*#	1.98±0.85#*
F	18	0	3	2	1	18	75.0%*#	5.75±1.35*#

*$P<0.05$, *VS control group*, #$P<0.05$, *VS model group*

Fig. 1: In vivo inhibition of stone formation in rats by *Persicaria capitata*. A: Renal H&E staining of the control group, 300×(n=12).
B: Renal H&E staining of the model group, 300×(n=12).
C: Renal H&E staining of the stone-discharge granule (PSKL) treatment group, 300×(n=12).
D: Renal H&E staining of the low-dose *Persicaria capitata* treatment group, 300×(n=12).
E: Renal H&E staining of the mid-dose *Persicaria capitata* treatment group, 300×(n=12).
F: Renal H&E staining of the high-dose *Persicaria capitata* treatment group, 300×(n=12).
G: Distribution and formation rate of stones in rats(n=12).

Additionally, compared to the control group, the model group displayed significantly more acidic urine ($P < 0.05$). Among the treatment groups, the urine pH of rats treated with *Persicaria capitata* was significantly increased ($P < 0.05$), with the ranking of pH values as follows: medium-dose *Persicaria capitata* > high-dose *Persicaria capitata* > low-dose *Persicaria capitata* > PSKL group (Fig. 2A). The model group had significantly higher urinary oxalate excretion compared to the control group ($P < 0.05$). however, urinary oxalate excretion was significantly reduced in the treatment groups compared to the model group, with the following ranking: high-dose *Persicaria capitata* > PSKL group > low-dose *Persicaria capitata* > medium-dose *Persicaria capitata*. This suggests that *Persicaria capitata* can effectively reduce urinary oxalate levels in rats with oxalate stones.

A

Group	Urine PH	Urinary oxalic acid (mg/L)	Urinary citric acid (mg/L)	Urine volume (mL)
A	7.61±0.44	1073.61±377.6	964.45±64.37	10.32±0.43
B	6.85±0.68*	2666.06±225.56*	233.15±20.69*	8.14±0.54*
C	7.3±0.29	1181.44±105.86*#	232.57±20.99*#	11.05±0.54*
D	7.68±0.48#	1151.84±151.34*#	645±115.34*#	12.72±0.84*#
E	7.87±0.36#	931.35±129.098*#	1107.41±89.12*#	12.94±0.33*#
F	7.83±0.55#	1544.28±113.58*#	402.29±40.65*#	13.74±0.64*#
F	*7.123*	*128.3*	*331.5*	*168.1*
P	*<0.05*	*<0.05*	*<0.05*	*<0.05*

*P<0.05, VS control group , #P<0.05, VS model group

B

Group	Urinary K (mmol/L)	Urinary Na (mmol/L)	Urinary Ca (mmol/L)	Urinary Mg (mmol/L)
A	58.03±7.41	22.58±0.23	0.88±0.05	7.7±0.26
B	145.26±7.89*	108.87±5.61*	1.21±0.08*	6.22±0.22*
C	109.94±5.37*#	70.39±2.43*#	0.84±0.08*#	10.7±0.56*#
D	163.25±12.39*#	97.66±1.18*#	0.54±0.04*#	12.38±0.31*#
E	63.13±7.49*#	48.54±4.55*#	0.63±0.03*#	14.8±0.45*#
F	83±2.47*#	29.87±1.6*#	0.86±0.07*#	8.69±0.15*#
F	*345.5*	*1341*	*153.6*	*884*
P	*<0.05*	*<0.05*	*<0.05*	*<0.05*

*P<0.05, VS control group , #P<0.05, VS model group

C

Group	Scr (umol/L)	Blood Ca (mmol/L)	Blood Mg (mmol/L)	Blood K (mmol/L)	Blood Na (mmol/L)
A	21.01±0.74	2.39±0.04	0.95±0.07	7.75±0.57	135.72±2.92
B	38.78±2.69*	2.41±0.04	0.95±0.05	7.75±0.48	133.77±2.29
C	32.97±3.13*#	2.42±0.06	0.92±0.07	7.76±0.55	136.49±2.81
D	30.13±1.58*#	2.43±0.04	0.94±0.06	7.56±0.54	134±2.78
E	30.66±2.89*#	2.43±0.05	0.94±0.06	7.72±0.36	134.25±2.57
F	33.85±2.69*#	2.43±0.04	0.97±0.06	7.97±0.47	135.49±2.81
F	*63.93*	*1.667*	*0.7892*	*0.7526*	*1.816*
P	*<0.05*	*0.1549*	*0.5612*	*0.5872*	*0.1217*

*P<0.05, VS control group , #P<0.05, VS model group

Fig. 2: Effects of *Persicaria capitata* on urine excretion and serum creatinine levels in kidney stone rats.
A: Urine pH, uric acid, citrate content, and urine volume in rats(n=12).
B: Urine potassium, sodium, calcium, and magnesium content in rats(n=12).
C: Serum creatinine, calcium, magnesium, potassium, and sodium levels in rats(n=12).

In terms of urinary citrate excretion, the model group showed significantly reduced excretion compared to the control group ($P < 0.05$). Urinary citrate excretion in the treatment groups was ranked as follows: medium-dose *Persicaria capitata* > low-dose *Persicaria capitata* > high-dose *Persicaria capitata* > PSKL group, suggesting that *Persicaria capitata* effectively increases urinary citrate levels in rats with oxalate stones.

In comparison of urine volume, the model group showed significantly reduced urine output compared to the control group ($P < 0.05$). The medium-dose and high-dose *Persicaria capitata* groups significantly

increased urine output compared to the model group, with the ranking as follows: high-dose *Persicaria capitata* > medium-dose *Persicaria capitata* > low-dose *Persicaria capitata* > PSKL group. This indicates that *Persicaria capitata* can effectively promote urine excretion.

Compared to the control group, the concentration of urinary cations in the model group was significantly increased ($P < 0.05$). Except for the low-dose *Persicaria capitata* group, all other treatment groups significantly reduced urinary potassium concentration (Fig. 2B). Additionally, compared to the model group, all treatment groups significantly reduced urinary sodium, calcium, and magnesium concentration.

No significant changes in blood potassium, calcium, sodium, or magnesium levels were observed between the model group and the control group ($P > 0.05$) (Fig. 2C), suggesting that the anti-stone effects of the treatments may not be related to these blood electrolytes, which are likely maintained due to the difficulty in disrupting blood homeostasis. However, compared to the model group, all treatment groups significantly reduced serum creatinine levels, the efficacy ranking of the treatments was as follows: high-dose *Persicaria capitata* > PSKL group > medium-dose *Persicaria capitata* > low-dose *Persicaria capitata*. This indicates that *Persicaria capitata* has a protective effect against calcium oxalate stones by reducing serum creatinine levels in rats.

3.2 Persicaria capitata alleviates oxidative stress in rat kidneys by modulating the antioxidant enzyme system and lipid oxidation metabolism.

Reactive oxygen species (ROS) detection in rat kidneys showed a significant increase in ROS levels in the model group, while *Persicaria capitata* treatment significantly reduced ROS levels, with the middle dose of *Persicaria capitata* showing superior effects compared to the PSKL (Fig. 3A and 3B). TUNEL staining results indicated that *Persicaria capitata* treatment significantly reduced the level of apoptosis in rat renal cells (Fig. 3C). We analyzed the metabolic differences in rat kidney tissues between the model group and the *Persicaria capitata* treatment group using metabolomics. Compared to the model group, the metabolite profile after *Persicaria capitata* treatment showed 241 upregulated metabolites and 128 downregulated metabolites (Fig. 3D). Principal Component Analysis (PCA) of the model and *Persicaria capitata* treatment groups is shown in Fig. 3E and 3F, and the interaction and clustering analysis of metabolites is presented in Fig. 3G and 3H. After *Persicaria capitata* treatment, significant changes were observed in metabolic pathways such as amino sugar and nucleotide sugar metabolism, fructose and mannose, and taurine and low taurine. Antioxidant carnitine metabolites, including carnitine C6:0, carnitine C20:2, carnitine C8-OH, carnitine C5:1, and carnitine C9:1-OH, were significantly increased. Oxidized lipid leukotrienes, such as D4 and trans-leukotriene D4, were significantly reduced, and oxidized lipids, including prostaglandin A2, prostaglandin B1, prostaglandin B2, and prostaglandin F2α, were also significantly reduced. Carbohydrate metabolites, such as lacto-N-tetraose, maltitol, and fructose, were significantly increased. Free fatty acids, including linoleic acid and ω-3 arachidonic acid, were elevated. Anti-inflammatory substances, such as taurocholic acid, were increased (Fig. 3I and 3J).

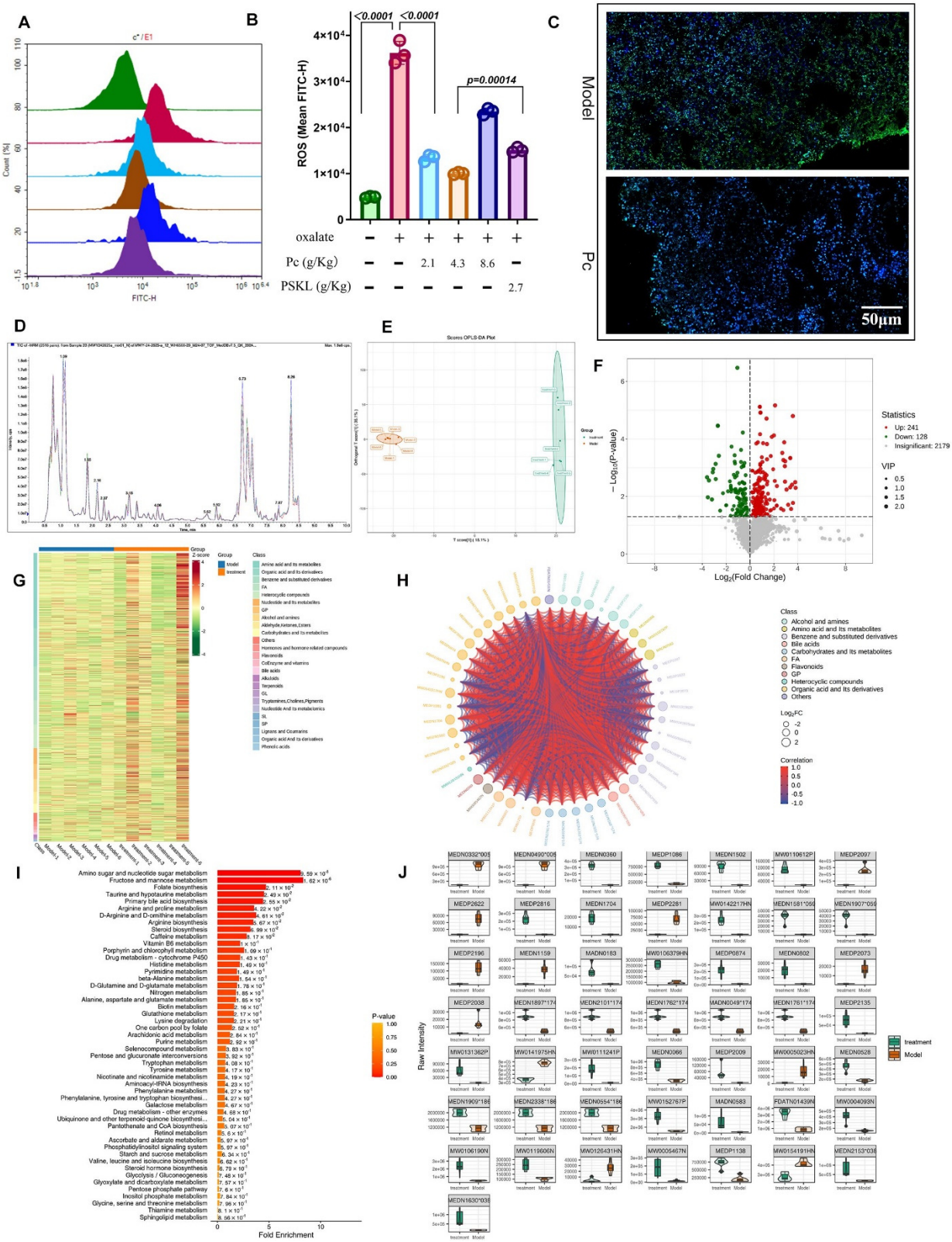

Fig. 3: Regulation of metabolic levels and reduction of oxidative stress in kidney stone rats by *Persicaria capitata*.
A-B: Level of reactive oxygen species (ROS) in the kidneys of stone rats(n=3). C: TUNEL staining of kidney sections from stone rats(n=3).
D: LC-MS analysis of metabolic differences between the model group and *Persicaria capitata* treatment group.
E: PCA plot of metabolic differences between the model group and *Persicaria capitata* treatment group.
F: Volcano plot of metabolic differences between the model group and *Persicaria capitata* treatment group.
G: Heatmap of metabolic differences between the model group and *Persicaria capitata* treatment group.
H: Interaction chord diagram of metabolic differences between the model group and *Persicaria capitata* treatment group.
I: Pathway diagram of metabolic differences between the model group and *Persicaria capitata* treatment group.
J: Top 50 metabolites with differences between the model group and *Persicaria capitata* treatment group.

3.3 Persicaria capitata significantly reduces oxidatives stress in a high oxalate-induced cellular injury model

To further evaluate the effects of *Persicaria capitata* on cellular oxidative stress in vitro, we first assessed its toxicity to renal cells. The results showed that *Persicaria capitata* at concentrations ranging from 0 to 400 mg/ml did not exhibit significant toxicity to HK-2 and NRK cells (Supplementary Fig. 1A). Reactive oxygen species (ROS) detection indicated that *Persicaria capitata* significantly reduced ROS accumulation induced by calcium oxalate (Fig. 4A and 4B). Transmission electron microscopy revealed that calcium oxalate caused mitochondrial swelling in HK-2 cells, which was alleviated by *Persicaria capitata* treatment (Fig. 4C). Additionally, *Persicaria capitata* significantly reduced lipid peroxidation caused by calcium oxalate (Fig. 4D), markedly increased SOD enzyme activity (Fig. 4E), and significantly enhanced ATP content in HK-2 cells (Fig. 4F). Cell apoptosis assays showed that calcium oxalate induced apoptosis in HK-2 cells, while *Persicaria capitata* treatment significantly reduced the proportion of apoptotic cells (Fig. 4G and 4H).

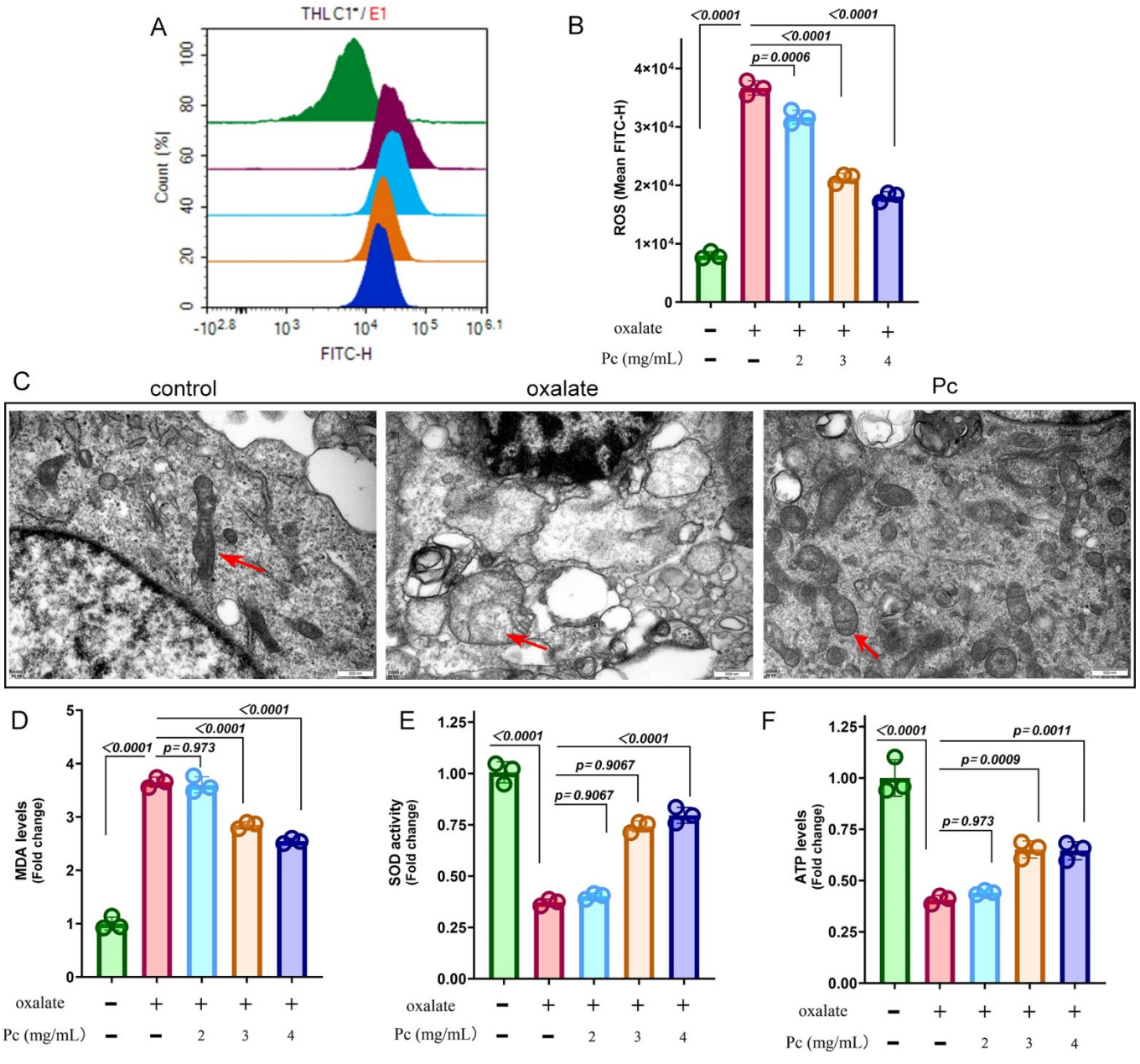

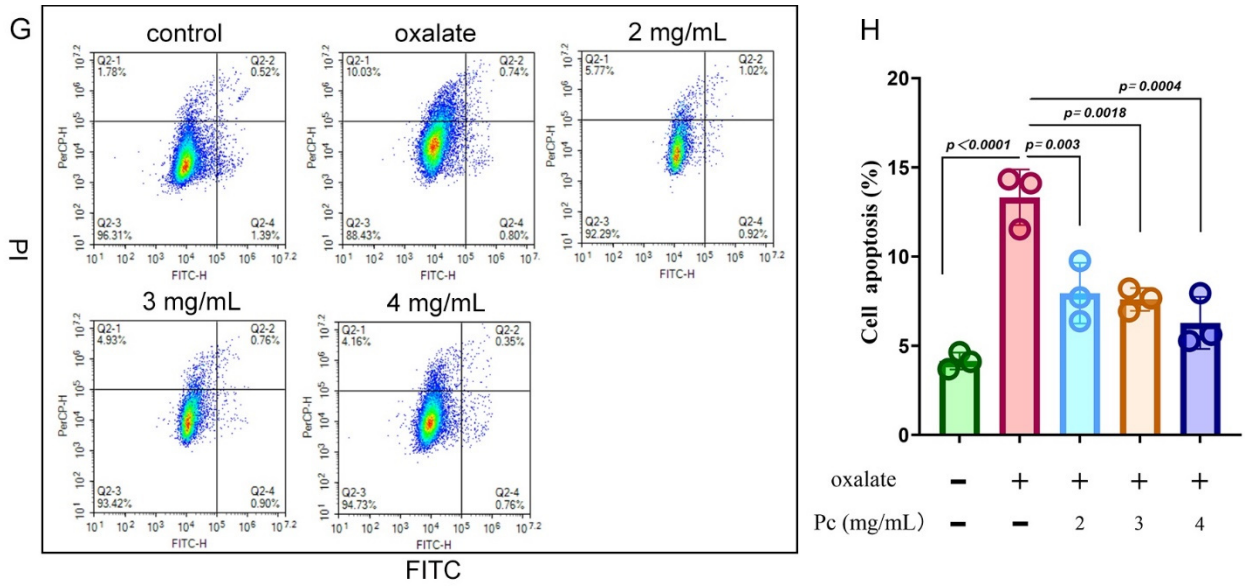

Fig. 4: In vitro reduction of oxidative stress induced by high oxalate by *Persicaria capitata* extract. A-B: Effect of *Persicaria capitata* treatment on reactive oxygen species (ROS) in HK-2 cells(n=3). C: Effect of *Persicaria capitata* treatment on mitochondrial morphology in HK-2 cells. D: Effect of *Persicaria capitata* treatment on MDA levels in HK-2 cells(n=3). E: Effect of *Persicaria capitata* treatment on SOD levels in HK-2 cells(n=3). F: Effect of *Persicaria capitata* treatment on ATP content in HK-2 cells(n=3). G-H: Effect of *Persicaria capitata* treatment on apoptosis in HK-2 cells(n=3); Oxalate concentration: 1 mmol/L; treatment time: 48 h.

3.4 Exploration of the pathways through which Persicaria capitata inhibits oxidative stress via transcriptomic sequencing and network pharmacology analysis

To further explore the mechanism by which *Persicaria capitata* alleviates kidney stone symptoms, we performed transcriptomic sequencing to analyze mRNA expression changes in the kidneys of control, model, and middle-dose *Persicaria capitata* treatment groups. The volcano plot of differential genes is shown in Fig. 5A, and KEGG enrichment analysis revealed significant changes in genes related to the PI3K-AKT and MAPK signaling pathways (Fig. 5B). Additionally, we analyzed the components of *Persicaria capitata* using LC-MS, as depicted in Fig. 5C. Initially, we screened the components of *Persicaria capitata*, retaining those with an OB value greater than 30% and a DL value greater than 0.18, as well as those reported to have good activity in the literature. The screening results are shown in Fig. 5D. Subsequently, we used network pharmacology methods to analyze the relationships between *Persicaria capitata* components and their targets, with target interactions illustrated in Fig. 5E. KEGG analysis also indicated significant changes in the MAPK signaling pathway, as shown in Fig. 5F and 5G. The relationship between *Persicaria capitata* and kidney stone-related targets is depicted in Fig. 5H.

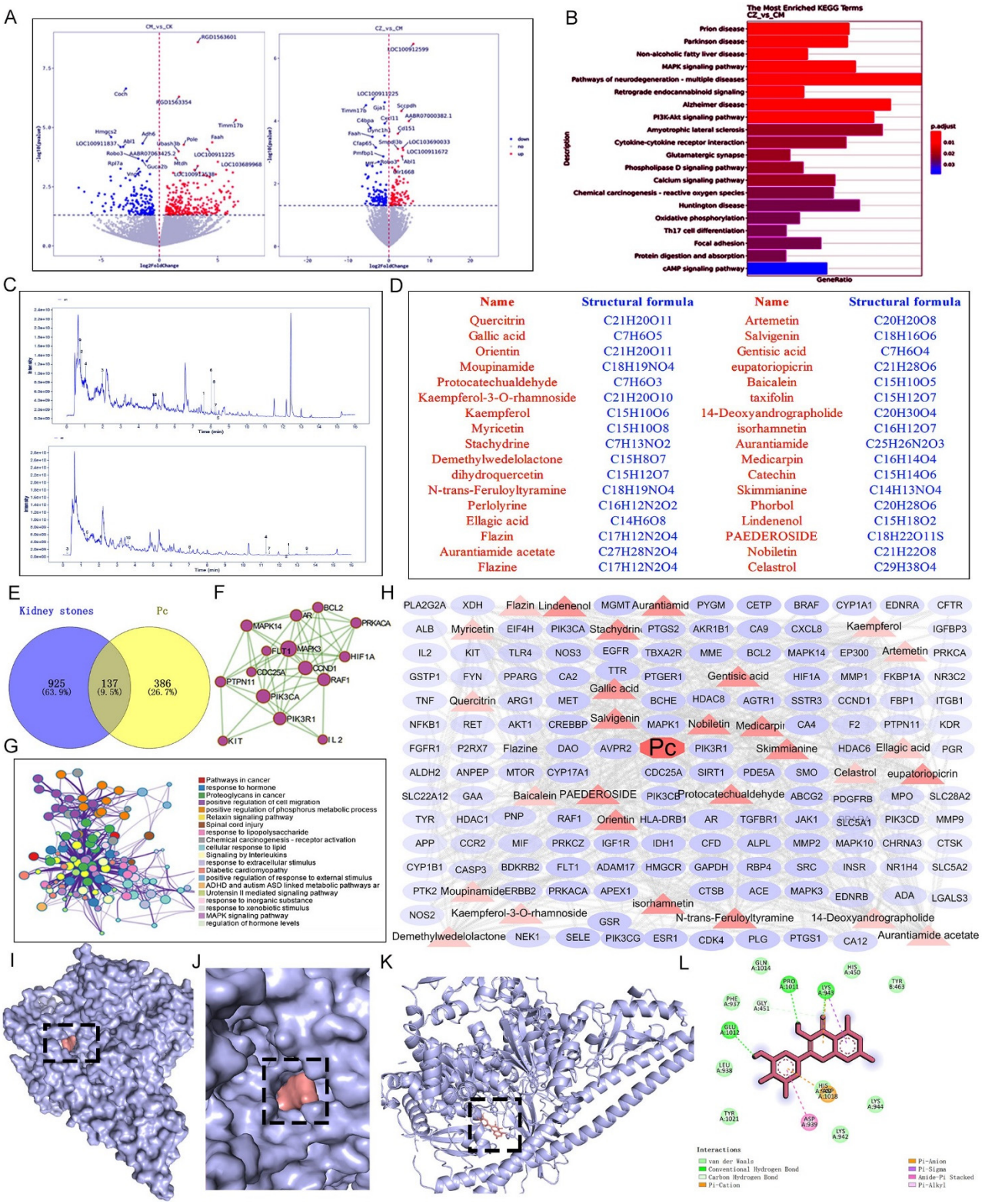

Fig. 5: Component analysis of *Persicaria capitata*; transcriptomic sequencing combined with network pharmacology analysis of potential pharmacological components and targets.

A: Volcano plots of transcriptomic sequencing in renal tissues of the control group, model group, and *Persicaria capitata* treatment group.

B: KEGG enrichment analysis of metabolic differences between the model group and *Persicaria capitata* treatment group.

C: LC-MS spectra of *Persicaria capitata* extract (negative and positive ion modes). D: Components of *Persicaria capitata* extract.

E: Network pharmacology analysis of common targets between kidney stones and *Persicaria capitata*.

F-G: KEGG enrichment analysis of common targets between kidney stones and *Persicaria capitata*.

H: Potential components and targets of *Persicaria capitata* in treating kidney stones. I-L: Molecular docking of Myricetin with PIK3CA in *Persicaria capitata*.

To further investigate how *Persicaria capitata* components regulate oxidative stress through their targets, we analyzed the core targets of *Persicaria capitata* for kidney stones and performed molecular docking of the top 10 targets with *Persicaria capitata* components. The results showed that the binding activity of Myricetin from *Persicaria capitata* with PIK3CA was strong (-7.95 kJ/mol), and the molecular docking results of Myricetin with PIK3CA are shown in Fig. 5I-5L.

3.5 Persicaria capitata alleviates calcium oxalate-induced oxidative stress in HK-2 cells by modulating the PIK3CA-ERK-NRF2 signaling pathway

Transcriptomic sequencing and network pharmacology analyses suggest that *Persicaria capitata* may inhibit renal cellular oxidative stress through the PIK3CA-ERK signaling pathway. To validate this hypothesis, we conducted immunohistochemical analyses to compare the expression levels of PIK3CA, ERK, NRF2, and OPN proteins in the kidneys of model and middle-dose *Persicaria capitata*-treated rats. The results showed that, compared to the model group, *Persicaria capitata* treatment significantly increased the expression of PIK3CA, ERK, and NRF2 proteins, while the expression of the renal injury marker OPN protein was significantly reduced (Fig. 6A). This suggests that *Persicaria capitata* may inhibit oxidative stress and kidney damage caused by oxalate stones via the PI3K signaling pathway. Additionally, we examined the expression of these proteins in the HK-2 high oxalate cell model. Compared to the model group, *Persicaria capitata* treatment significantly increased the expression of PIK3CA and ERK proteins (Fig. 6B and 6C), while NRF2, SOD, and HO-1 protein levels were also significantly elevated, and NOX2, NOX4, and OPN proteins were significantly decreased (Fig. 6D and 6E). These results indicate that *Persicaria capitata* may alleviate oxidative stress by upregulating PIK3CA, enhancing ERK expression, and further increasing NRF2 expression.

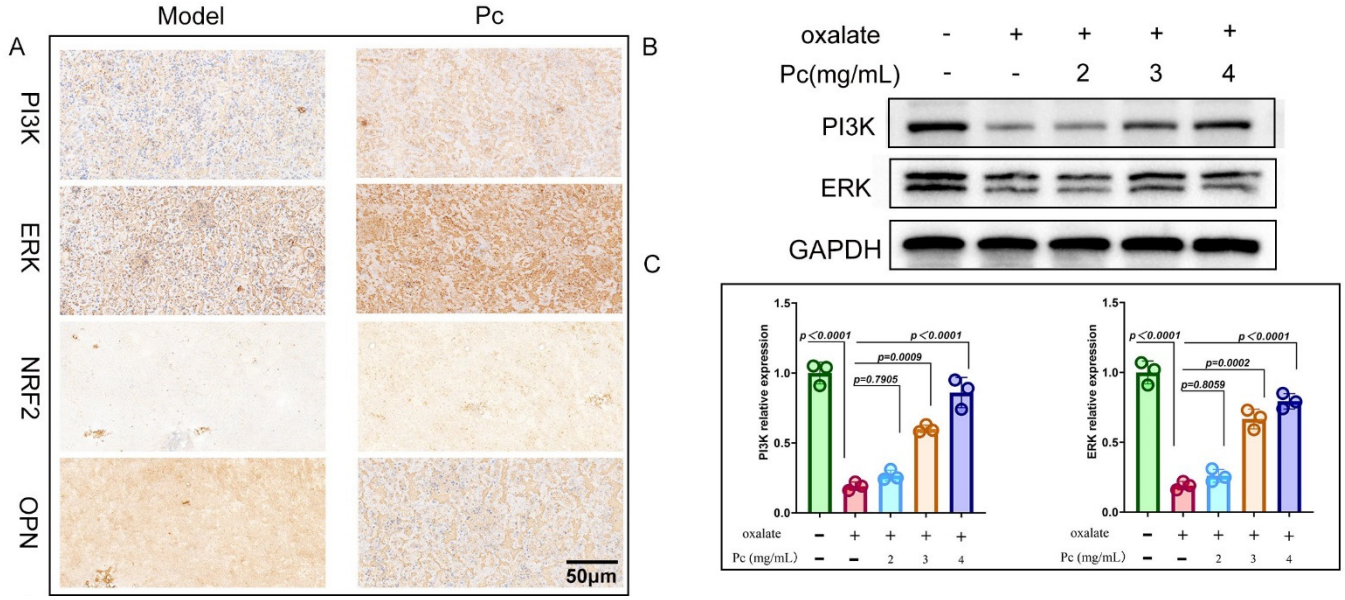

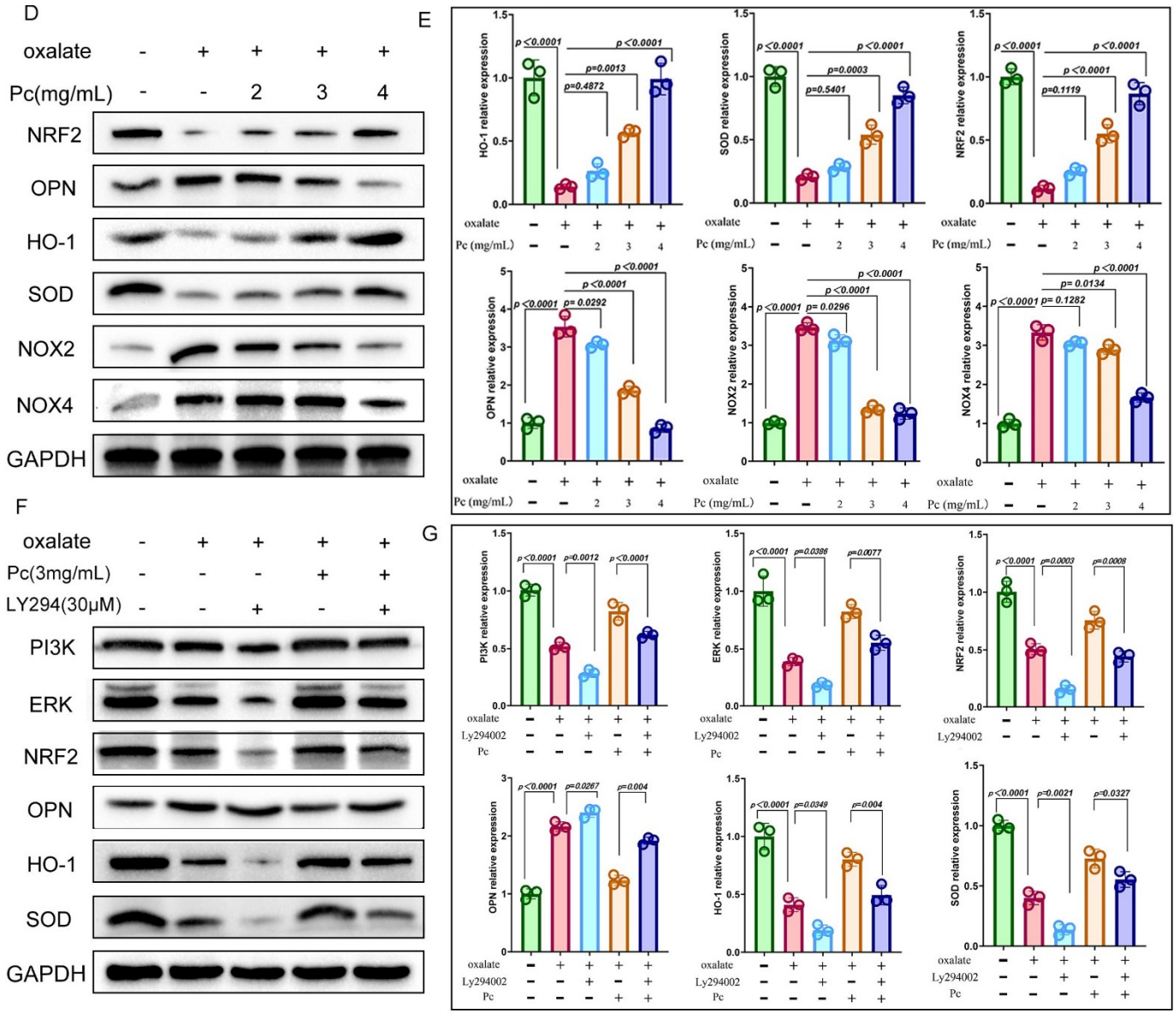

Fig. 6: *Persicaria capitata* extract reduces oxidative stress levels through the PI3K-ERK-NRF2 pathway in vitro and in vivo.
A: Immunohistochemical analysis of PI3K, ERK, NRF2, and OPN protein expression levels in renal tissues of the model and *Persicaria capitata* treatment groups(n=3).
B-C: Effect of *Persicaria capitata* on PI3K and ERK protein expression levels in HK-2 cells(n=3).
D-E: Effect of *Persicaria capitata* on NRF2, OPN, HO-1, SOD, NOX2, and NOX4 protein expression levels in HK-2 cells(n=3).
F-G: Effect of PI3K inhibitor combined with *Persicaria capitata* treatment on PI3K, ERK, NRF2, OPN, HO-1, and SOD protein expression levels in HK-2 cells(n=3). oxalate concentration: 1 mmol/L; treatment time: 48 h.

To further elucidate the role of PIK3CA in *Persicaria capitata*-mediated oxidative stress inhibition, we used LY294002 (a PI3K inhibitor) to observe its effects on downstream ERK and NRF2 protein expression levels. The results showed that, compared to the model group, LY294002 treatment significantly reduced the expression levels of PIK3CA, ERK, SOD, NRF2, and HO-1 proteins, and significantly increased the expression of OPN protein. In contrast, the combination of *Persicaria capitata* and LY294002 significantly increased the expression levels of PIK3CA, SOD, ERK, and NRF2 proteins, while significantly reducing the expression of OPN protein (Fig. 6F and 6G). These findings suggest that PIK3CA may be a key target of *Persicaria capitata* in inhibiting renal oxidative stress.

3.6 Myricetin directly binds to PIK3CA

To further identify the key substances in *Persicaria capitata* responsible for its antioxidant effects, we performed a combined analysis of *Persicaria capitata* components, transcriptomic sequencing data, and network pharmacology data. Molecular docking results indicated that Myricetin has good binding potential with PIK3CA. To assess this binding potential, we employed Cellular Thermal Shift Assay (CETSA), Drug Affinity Responsive Target Stability (DARTS), and molecular dynamics simulations. CETSA results showed that after co-incubation of Myricetin with total HK-2 cell proteins, the degradation temperature of PIK3CA protein increased by 3-6 ℃ (Fig.7A and 7B). DARTS results indicated that after Pronase treatment, the degradation level of PIK3CA protein in the Myricetin treatment group was significantly reduced (Fig. 7C and 7D). Molecular dynamics simulation results showed that the RMSD value of the Myricetin-PIK3CA complex fluctuated significantly within 40 ns, then stabilized, indicating structural stability of the complex (Fig. 7E). During the binding process, the RMSF value was larger in the 850-900 amino acid sequence range, suggesting good flexibility of the protein in this region (Fig. 7F). As the protein and small molecule stabilized during the simulation, both the Rg and SASA values showed a decreasing trend (Fig. 7G and 7H). Throughout the 100 ns simulation, the complex maintained 2-7 hydrogen bonds for most of the time (Fig. 7I). The total binding energy was (-27.89 ± 1.94) kcal/mol (Fig.7J). Based on the above results， indicating strong affinity between Myricetin and PIK3CA.

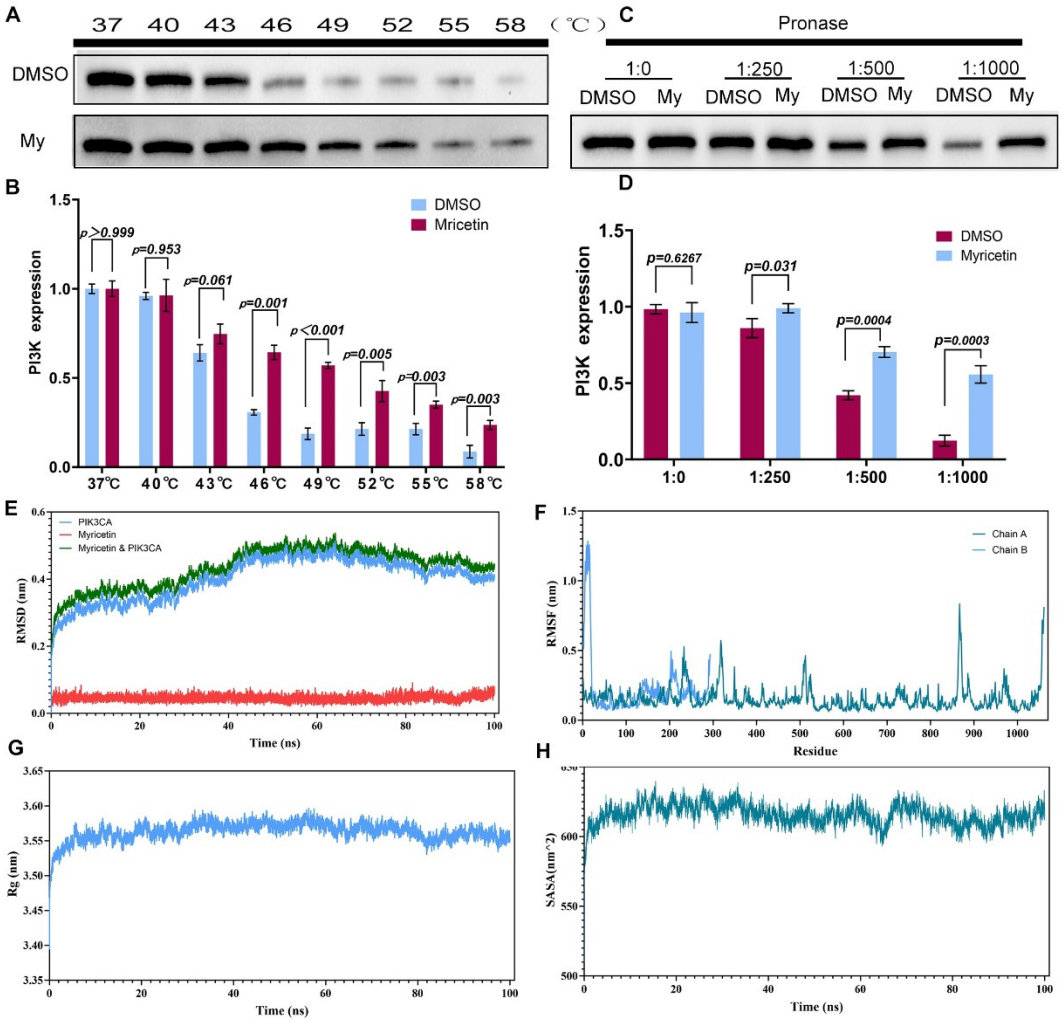

I

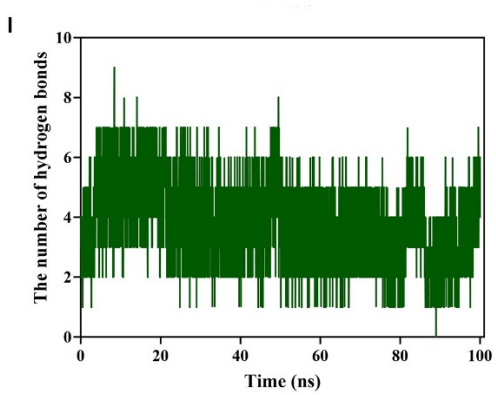

J

Energy	Complex(Kcal/mol)
ΔVDWAALS	-35.15 ± 1.03
ΔEEL	-43.35 ± 1.55
ΔEGB	56.01 ± 0.56
ΔESURF	-5.40 ± 0.01
ΔGGAS	-78.50 ± 1.86
ΔGSOLV	50.61 ± 0.56
ΔTOTAL	-27.89 ± 1.94

Fig. 7: Binding of the pharmacological component Myricetin to PIK3CA in *Persicaria capitata* extract. A-B: CETSA-WB experiments assessing the binding potential of Myricetin with PIK3CA(n=3). C-D: DARTS-WB experiments assessing the binding potential of Myricetin with PIK3CA(n=3). E: Molecular dynamics simulation of RMSD values for the PIK3CA-Myricetin complex. F: Molecular dynamics simulation of RMSF values for the PIK3CA-Myricetin complex. G-H: Molecular dynamics simulation of Rg and SASA values for the PIK3CA-Myricetin complex. I: Number of hydrogen bonds in the PIK3CA-Myricetin complex during simulation. J: Energy analysis of the PIK3CA-Myricetin complex.

3.7 Myricetin, an active component of Persicaria capitata, significantly reduces oxidative stress in a high oxalate cell injury model

To further explore the role of Myricetin in *Persicaria capitata's* inhibition of kidney stone oxidative stress, we first assessed the cytotoxicity of Myricetin. The results showed that, within the concentration range of 0-50 μM, Myricetin did not cause significant toxicity to HK-2 cells (Supplementary Fig. 2B). Subsequently, we evaluated the potential of Myricetin to inhibit oxidative stress. The results showed that Myricetin significantly inhibited the increase in reactive oxygen species (ROS) levels induced by calcium oxalate in HK-2 cells (Fig. 8A and 8B). After inhibiting the PI3K signaling pathway, the ROS inhibition capacity of Myricetin was significantly reduced (Fig. 8C and 8D). We also observed that Myricetin protected cell morphology in the high oxalate cell injury model (Supplementary Fig. 1C). These results suggest that Myricetin may inhibit oxidative stress through the PI3K signaling pathway. In the high oxalate cell injury model, Western blot results showed that compared to the model group, Myricetin treatment significantly increased the expression levels of PIK3CA, ERK, NRF2, HO-1, and SOD proteins, while significantly reducing the expression level of OPN protein (Fig. 8E and 8F). This suggests that Myricetin may inhibit oxidative stress by modulating the PI3K-ERK-NRF2 signaling pathway.

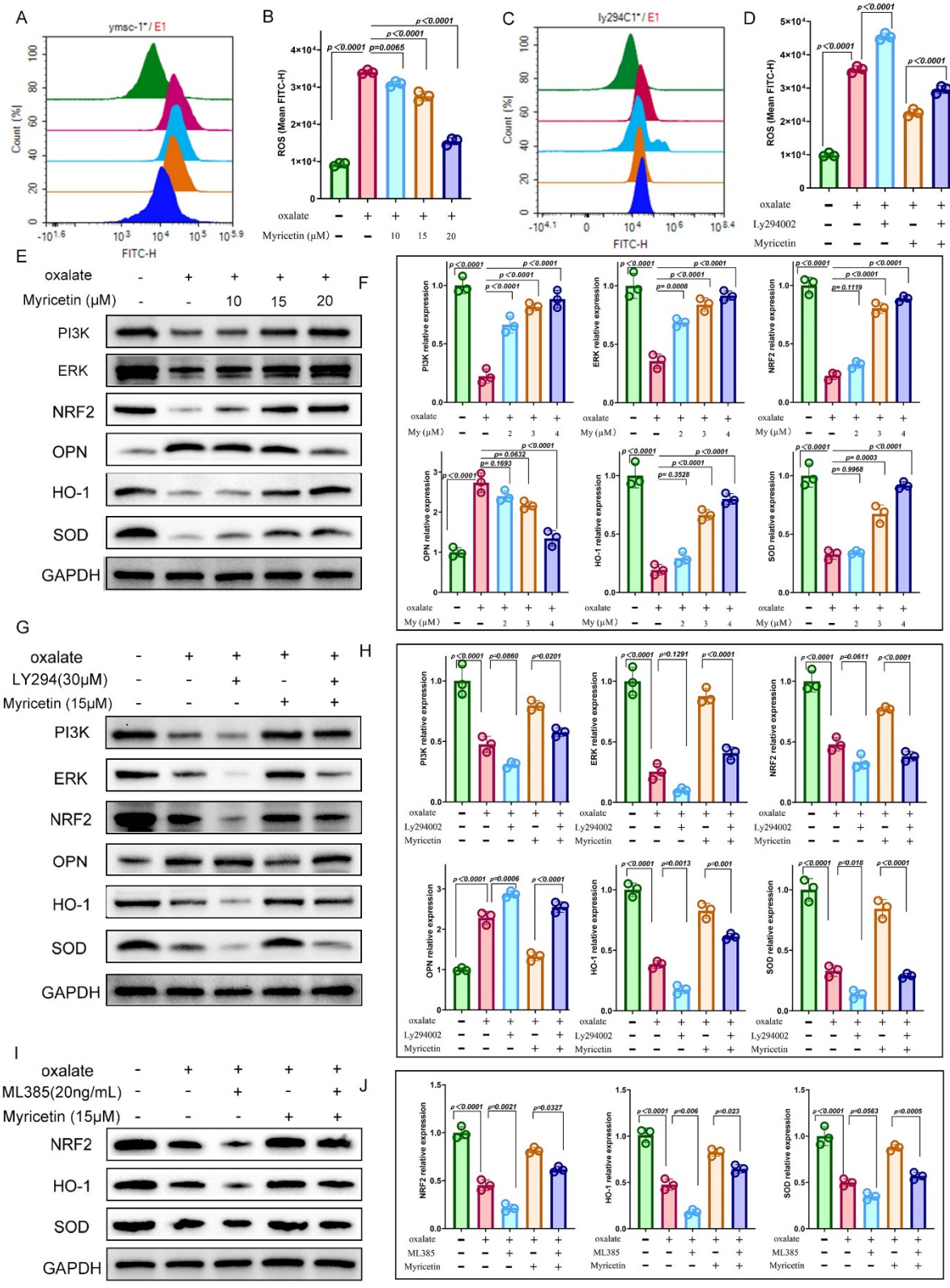

Fig. 8: Myricetin from *Persicaria capitata* extract inhibits oxidative stress in HK-2 cells through the PI3K-ERK-NRF2 pathway.

A-B: Effect of Myricetin treatment on ROS levels in HK-2 cells(n=3).

C-D: Effect of PI3K inhibitor combined with Myricetin treatment on ROS levels in HK-2 cells(n=3).

E-F: Effect of Myricetin on PI3K, ERK, NRF2, OPN, HO-1, and SOD protein expression levels in HK-2 cells(n=3).

G-H: Effect of PI3K inhibitor combined with Myricetin treatment on PI3K, ERK, NRF2, OPN, HO-1, and SOD protein expression levels in HK-2 cells(n=3).

I-J: Effect of NRF2 inhibitor combined with Myricetin treatment on NRF2, HO-1, and SOD protein expression levels in HK-2 cells(n=3). Oxalate concentration: 1 mmol/L; treatment time: 48 h.

3.8 Myricetin, an active component of Persicaria capitata, inhibits excessive oxidative stress in the high oxalate cell injury model via targeting the PIK3CA-ERK-NRF2 signaling pathway

Based on the results, there is strong evidence that Myricetin may be a key pharmacological component in *Persicaria capitata* that regulates PIK3CA and NRF2 to inhibit renal cellular oxidative stress. To verify this hypothesis, we intervened in calcium oxalate-treated HK-2 cells with LY294002 and ML385 (NRF2 inhibitors). The results showed that, compared to the LY294002 alone group, the Myricetin- LY294002 group had significantly increased levels of PIK3CA, ERK, NRF2, SOD and HO-1 proteins, while the OPN protein level was significantly reduced (Fig. 8G and 8H). Compared to the model group, the ML385 intervention group showed significantly reduced levels of NRF2, SOD and HO-1, protein; however, the Myricetin-ML385 group had significantly increased levels of NRF2, HO-1, and SOD proteins compared to the ML385 group (Fig. 8I and 8J). These results indicate that Myricetin exhibits functionality similar to that of *Persicaria capitata* by binding to PIK3CA, promoting its expression, increasing ERK expression, and further enhancing NRF2 expression to inhibit oxidative stress and protect normal kidney cell function, Myricetin is a potent component of touhualiao in inhibiting kidney stones.

It is noteworthy that, in addition to Myricetin, we also analyzed other components of *Persicaria capitata*, such as Orientin, for their potential to inhibit oxidative stress. The results showed that after combined treatment of Myricetin and Orientin in HK-2 cells, the expression levels of NRF2 and SOD proteins were significantly higher than those in the Myricetin alone group, while the expression level of OPN protein was significantly lower (Supplementary Fig. 1D and 1E). Therefore, we believe that the inhibitory function of *Persicaria capitata* on oxidative stress may be achieved through the synergistic effects of multiple targets and components. This synergistic effect can reduce oxidative stress levels in kidney stones, inhibit the formation of oxalate stones, and thus protect the normal function of kidney cells. The mechanism of action of *Persicaria capitata* on inhibiting oxidative stress is shown in Fig. 9

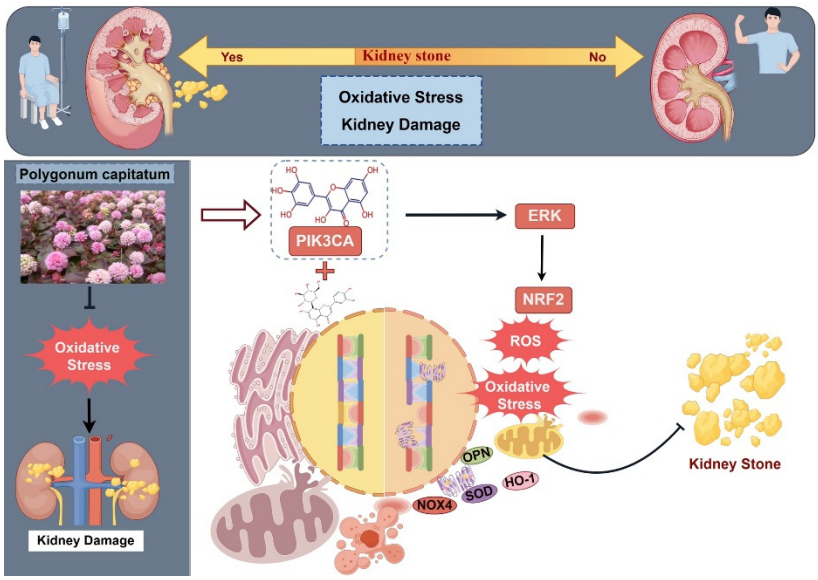

Fig. 9: Schematic diagram of the mechanism of *Persicaria capitata* on inhibiting kidney stone formation. The extract of *Polygonum capitatum* alleviates hyperoxaluria-induced oxidative stress by targeting the PI3K-ERK-NRF2 signaling pathway.
Diagram of molecular mechanisms.

4. Discussion

The characteristics of calcium oxalate stones suggest that the early stage is the optimal time for intervention, as this is when crystals begin to form and adhere to endothelial cells, but have not yet developed into larger, harder solids. To more comprehensively assess the preventive or therapeutic potential of *Persicaria capitata* for calcium oxalate stones, we implemented a simultaneous modeling and treatment approach in the kidney oxalate stone rat model, conducting modeling in the morning and drug intervention in the afternoon. Additionally, to evaluate its efficacy, we used a PSKL as a positive control. The results indicated that the mid-dose *Persicaria capitata* treatment inhibited calcium oxalate stones in rats even more effectively than the PSKL (Fig. 1D and 1F).

Once stones start to form, their continued growth requires two conditions: an acidic urine environment to provide more oxalate ions and a high concentration of cations in the urine to provide ligands for oxalate ions. In this study, we assessed urine pH, cation concentration, and oxalate concentration in the *Persicaria capitata*-treated calcium oxalate rat model. The results showed that both *Persicaria capitata* and PSKL increased the urine pH in rats (Fig. 2A) and reduced the concentrations of sodium, magnesium, calcium, potassium, and oxalate. Although the exact mechanisms by which these ions influence stone formation are not fully understood, these findings could provide a theoretical basis for clinical treatment of kidney stones. Interestingly, *Persicaria capitata* treatment also significantly increased the concentration of citrate in rat urine. Citrate interacts with calcium ions to form soluble calcium citrate, which lowers the saturation of calcium salts in urine, inhibits the crystallization, growth, and aggregation of calcium oxalate and calcium phosphate, and increases urine pH (resulting in alkaline urine), thus aiding in the dissolution of acidic stones. However, no meaningful changes in the concentrations of sodium, magnesium, calcium, and potassium ions were detected in the serum of *Persicaria capitata*-treated rats. This discrepancy might be due to the substantial differences between blood and urine environments, or because blood homeostasis is more strictly regulated and less prone to change. Elevated serum creatinine is a recognized marker of renal injury, and we observed a significant decrease in creatinine in the blood of *Persicaria capitata*-treated rats, suggesting that *Persicaria capitata* might protect renal cell function and reduce kidney damage probability by inhibiting stone formation, potentially through reducing oxidative stress in renal epithelial cells and maintaining mitochondrial function[26-27]. Additionally, we observed better glucose metabolism in the kidneys of *Persicaria capitata*-treated rats compared to the model group, with significantly increased levels of antioxidant carnitine metabolites and decreased levels of oxidative lipid leukotriene D4 and trans-leukotriene D4 (Fig. 3J).

LC-MS analysis of *Persicaria capitata* components revealed rich antioxidant activity, including Myricetin, quercetin, and Orientin. Myricetin, widely present in various natural plants, exhibits excellent antioxidant properties and can inhibit inflammation[28], protect against kidney damage, and support cardiovascular health[29-31]. Myricetin reduces inflammation by inhibiting the JAK/STAT1 and NOX2/p47 pathways, which are involved in NADPH oxidase-dependent ROS production[32], and generally acts

through MAPK, NRF2, and PI3K signaling pathways[33-36]. In our study, Myricetin significantly inhibited calcium oxalate-induced oxidative stress in HK-2 cells in vitro, indicating that it might be a key pharmacological component of *Persicaria capitata*. Quercetin can inhibit inflammatory responses by modulating the HSP90/NRF2 pathway and counteracting age-related ovarian reserve depletion[37-38], as well as controlling glucose uptake, mitochondrial biogenesis, and protein synthesis through PI3K/AKT and MAPK pathways[39-40]. In addition, Orientin has good antioxidant function, and its mechanism is related to the downregulation of oxidative stress mediated endoplasmic reticulum stress and mitochondrial dysfunction by ampk/sirt1 pathway[41-42].Our study also found that Myricetin and Orientin promoted the expression of NRF2 and HO-1 while inhibiting OPN expressions, alleviating oxidative stress in HK-2 cells. NRF2 is a transcription factor that plays a pivotal role in regulating cellular oxidative stress[43]. By modulating the expression of HO-1, NRF2 can enhance cellular antioxidant function, thereby mitigating cellular damage[44]. Strategies targeting the Nrf2-HO-1 signaling pathway to enhance cellular antioxidant capacity and alleviate cellular injury have been extensively elucidated[45-46].

In our study, we identified that the *Persicaria capitata* contains not only excellent antioxidant components such as Myricetin, Orientin, and Quercetin, but also compounds such as gallic acid, kaempferol, and ellagic acid. Among these, gallic acid has been widely confirmed to be present in a variety of plants and is known for its blood glucose-lowering and antioxidant properties[47-48]. Kaempferol exhibits potential in anti-atherosclerotic, anti-inflammatory, and antioxidant activities[49-50]. Ellagic acid has increasingly come into the focus of researchers for its potential roles in anti-aging and antitumor activities[51-52].

The close relationship between cellular oxidative stress and apoptosis, upon cellular stimulation, oxidative stress levels surge dramatically[52]. However, the cellular antioxidant system can neutralize reactive oxygen species (ROS) within a certain threshold. When the cellular antioxidant capacity is insufficient to counteract the rapid increase in ROS over a short period, the expression of NRF2 is suppressed, leading to an increase in the expression levels of the pro-apoptotic regulator Bax and a concomitant decrease in Bcl-2, thereby triggering apoptotic events[53-54]. We found that the extract of *Persicaria capitata* can effectively reduce the oxidative stress induced by high levels of oxalate, thereby reduceing apoptosis in renal tubular epithelial cells. In addition, we have discovered that Myricetin can bind with PI3KC, enhancing the expression levels of NRF2 to suppress excessive oxidative stress, thereby inhibiting the formation rate of kidney stones and reducing renal cell damage. This process is also accompanied by the suppression of inflammatory responses. Oxidative stress is regarded as an imbalance between the generation of reactive oxygen species (ROS) and the protective mechanisms that eliminate ROS, which may lead to inflammation[55-56]. Consequently, promoting the expression levels of NRF2 to inhibit cellular ROS has also become an effective strategy for anti-inflammatory purposes[57].

Network pharmacology and transcriptomic results pointed towards the PI3K and MAPK signaling pathways. Based on existing literature, we hypothesized that "Myricetin in *Persicaria capitata* targets

PIK3CA, further regulates ERK-mediated oxidative stress to reduce oxidative stress." To test this hypothesis, we employed molecular docking, molecular dynamics, and molecular thermodynamics to assess the binding potential of Myricetin to the target. The results showed that Myricetin has a strong affinity for PIK3CA. Further intervention with the PI3KCA inhibitor LY294002 in the calcium oxalate cell model led to decreased ERK protein expression levels. ERK activation of NRF2 to inhibit oxidative stress has been widely reported[58-59]. We also used NRF2 inhibitors for intervention; compared to the model group, the ML385 intervention group showed significantly reduced NRF2 and HO-1 levels and decreased SOD protein levels, whereas the Myricetin-ML385 group showed significantly increased levels of NRF2, SOD, and HO-1 proteins. This indicates that NRF2 is one of the key targets for Myricetin in inhibiting oxidative stress induced by high oxalate.

Exploration of the synergistic effects of *Persicaria capitata*'s pharmacological components revealed that the combination of Myricetin and Orientin was more effective in the calcium oxalate cell model than single treatments. Compared to the Myricetin-alone group, the combination treatment significantly increased NRF2, HO-1, and SOD protein levels, and reduced OPN protein levels. This suggests that *Persicaria capitata* may exert its therapeutic effects on calcium oxalate stones through a multi-component and multi-target synergistic mechanism.

In summary, our study indicates that *Persicaria capitata* inhibits calcium oxalate stone formation through a synergistic effect of multiple components and targets. After confirming *Persicaria capitata*'s therapeutic potential both in vitro and in vivo, we explored its specific pharmacological components and obtained interesting results. However, understanding of *Persicaria capitata* remains limited, and further multi-faceted analysis of its component-target relationships is necessary. As pharmacology rapidly advances, integrating serum pharmacology with transcriptomics and proteomics is crucial for analyzing traditional medicine signaling pathways. Additionally, studying small molecule-protein affinities using molecular thermodynamics techniques like SPR and MST is essential. Revealing new mechanisms of kidney stone formation is also significant for clinical treatment. After identifying key targets, structural pharmacology approaches should be used to design target-specific inhibitors to improve drug efficacy and reduce toxicity.

In conclusion, this study reveals that *Persicaria capitata* inhibits the formation of calcium oxalate stones and alleviates kidney damage through a multi-component and multi-target synergistic effect. Specifically, the active component Myricetin in *Persicaria capitata* binds to PIK3CA, increases ERK expression levels, and further suppresses excessive oxidative stress induced by high oxalate, thereby slowing stone formation and mitigating kidney damage caused by calcium oxalate stones. However, further research on other pharmacological components in *Persicaria capitata* is necessary to explore their full potential.

5. Conclusion

Persicaria capitata inhibits the formation of oxalate stones through a multi-component and multi-target synergistic effect. Specifically, the effective component Myricetin in *Persicaria capitata* binds to PIK3CA,

increases ERK expression levels, further reduces cellular oxidative stress, thus inhibiting oxalate stone formation and alleviating kidney damage caused by oxalate stones.

Conflict of interest

The authors declare that there is no conflict of interest in relation to this work.

Acknowledgments

This research was funded by the Guizhou Province Science and Technology Innovation Talent Team (CXTD[2023]011). The National Natural Science Foundation of China (81873608). The National Natural Science Foundation of China (82160551); the Talent Fund of Guizhou Provincial People ' s Hospital ([2023]-17). And the Second Batch of First-class Discipline Construction Projects in Guizhou Province "Ecology of Guiyang University".

References

[1] Peerapen, P. and V. Thongboonkerd, Kidney Stone Prevention. Adv Nutr, 14 (2023) 555-569. https://doi.org/10.1016/j.advnut.2023.03.002.

[2] Thongprayoon, C., A.E. Krambeck, and A.D. Rule, Determining the true burden of kidney stone disease. Nat Rev Nephrol, 16 (2020) 736-746. https://doi.org/10.1038/s41581-020-0320-7.

[3] Khan, S.R., M.S. Pearle, W.G. Robertson, et al., Kidney stones. Nat Rev Dis Primers, 2 (2016) 16008. https://doi.org/10.1038/nrdp.2016.8.

[4] Chen, T., B. Qian, J. Zou, et al., Oxalate as a potent promoter of kidney stone formation. Front Med (Lausanne), 10 (2023) 1159616. https://doi.org/10.3389/fmed.2023.1159616.

[5] Hawkins-van der Cingel, G., S.B. Walsh, K.U. Eckardt, et al., Oxalate Metabolism: From Kidney Stones to Cardiovascular Disease. Mayo Clin Proc, 99 (2024) 1149-1161. https://doi.org/10.1016/j.mayocp.2024.02.006.

[6] Deng, J., B. Yu, Z. Chang, et al., Cerium oxide-based nanozyme suppresses kidney calcium oxalate crystal depositions via reversing hyperoxaluria-induced oxidative stress damage. J Nanobiotechnology, 20 (2022) 516. https://doi.org/10.1186/s12951-022-01726-w.

[7] Xiong, J., L. Ran, Y. Zhu, et al., DUSP2-mediated inhibition of tubular epithelial cell pyroptosis confers nephroprotection in acute kidney injury. Theranostics, 12 (2022) 5069-5085. https://doi.org/10.7150/thno.72291.

[8] Kumar, P., E. Laurence, D.K. Crossman, et al., Oxalate disrupts monocyte and macrophage cellular function via Interleukin-10 and mitochondrial reactive oxygen species (ROS) signaling. Redox Biol, 67 (2023) 102919. https://doi.org/10.1016/j.redox.2023.102919.

[9] Ming, S., J. Tian, K. Ma, et al., Oxalate-induced apoptosis through ERS-ROS-NF-kappaB signalling pathwayin renal tubular epithelial cell. Mol Med, 28 (2022) 88. https://doi.org/10.1186/s10020-022-00494-5.

[10] Sun, Y., X. Ge, X. Li, et al., High-fat diet promotes renal injury by inducing oxidative stress and mitochondrial dysfunction. Cell Death Dis, 11 (2020) 914. https://doi.org/10.1038/s41419-020-03122-4.

[11] Assimos, D.G., Re: miR-155-5p Promotes Oxalate- and Calcium-Induced Kidney Oxidative Stress Injury by Suppressing MGP Expression. J Urol, 204 (2020) 381. https://doi.org/10.1097/JU.0000000000001112.03.

[12] Albert, A., V. Tiwari, E. Paul, et al., Expression of heterologous oxalate decarboxylase in HEK293 cells confers protection against oxalate induced oxidative stress as a therapeutic approach for calcium oxalate stone disease. J Enzyme Inhib Med Chem, 32 (2017) 426-433. https://doi.org/10.1080/14756366.2016.1256884.

[13] Gao, X., B. Lin, C. Chen, et al., Lycopene from tomatoes and tomato products exerts renoprotective effects by ameliorating oxidative stress, apoptosis, pyroptosis, fibrosis, and inflammatory injury in calcium oxalate nephrolithiasis: the underlying mechanisms. Food Funct, 15 (2024) 4021-4036. https://doi.org/10.1039/d4fo00042k.

[14] Guo, J.M., H.J. Xing, J.Z. Cai, et al., H(2)S exposure-induced oxidative stress promotes LPS-mediated hepatocyte autophagy through the PI3K/AKT/TOR pathway. Ecotoxicol Environ Saf, 209 (2021) 111801. https://doi.org/10.1016/j.ecoenv.2020.111801.

[15] Huang, L., D. Zhan, Y. Xing, et al., FGL2 deficiency alleviates maternal inflammation-induced blood-brain barrier damage by blocking PI3K/NF-kappaB mediated endothelial oxidative stress. Front Immunol, 14 (2023) 1157027. https://doi.org/10.3389/fimmu.2023.1157027.

[16] Bae, T., S.P. Hallis, and M.K. Kwak, Hypoxia, oxidative stress, and the interplay of HIFs and NRF2 signaling in cancer. Exp Mol Med, 56 (2024) 501-514. https://doi.org/10.1038/s12276-024-01180-8.

[17] Vanhaesebroeck, B., L. Stephens, and P. Hawkins, PI3K signalling: the path to discovery and understanding. Nat Rev Mol Cell Biol, 13 (2012) 195-203. https://doi.org/10.1038/nrm3290.

[18] Lin, X., W. Wang, X. Chang, et al., ROS/mtROS promotes TNTs formation via the PI3K/AKT/mTOR pathway to protect against mitochondrial damages in glial cells induced by engineered nanomaterials. Part Fibre Toxicol, 21 (2024) 1. https://doi.org/10.1186/s12989-024-00562-0.

[19] Deng, S., G. Dai, S. Chen, et al., Dexamethasone induces osteoblast apoptosis through ROS-PI3K/AKT/GSK3beta signaling pathway. Biomed Pharmacother, 110 (2019) 602-608. https://doi.org/10.1016/j.biopha.2018.11.103.

[20] Khan, S.R., Reactive oxygen species as the molecular modulators of calcium oxalate kidney stone formation: evidence from clinical and experimental investigations. J Urol, 189 (2013) 803-11. https://doi.org/10.1016/j.juro.2012.05.078.

[21] Selvam, R., Calcium oxalate stone disease: role of lipid peroxidation and antioxidants. Urol Res, 30 (2002) 35-47. https://doi.org/10.1007/s00240-001-0228-z.

[22] Wu, F. and Z. You, Illustrated book of common garden plant identification. 2010: Illustrated book of common garden plant identification.

[23] Yan, P. and Y. Xia, Strange Chinese herbal medicine · unilateral prescription. Volume 4. 2016: Strange Chinese herbal medicine · unilateral prescription. Volume 4.

[24] XIE, X., Effect of hot leaching granules on postoperative stone expulsion effect and urinary tract infection in patients with kidney stones. Chinese Practical Medicine, 21 (2021) 38-39. https://doi.org/10.13638/j.issn.1671-4040.2021.21.017.

[25] Wei, L. and B. Yu, Observation of the effects of hot leaching granules on the prevention of urinary tract infection after kidney stone surgery, and the effects of stone induction and pain relief. Chinese Journal of Traditional Chinese Medicine, 35 (2017) 766-768. https://doi.org/10.13193/j.issn.1673-7717.2017.03.073.

[26] Rossiter, A., A. La, J.L. Koyner, et al., New biomarkers in acute kidney injury. Crit Rev Clin Lab Sci, 61 (2024) 23-44. https://doi.org/10.1080/10408363.2023.2242481.

[27] Cai, F., D. Li, Y. Xie, et al., Sulfide:quinone oxidoreductase alleviates ferroptosis in acute kidney injury via ameliorating mitochondrial dysfunction of renal tubular epithelial cells. Redox Biol, 69 (2024) 102973. https://doi.org/10.1016/j.redox.2023.102973.

[28] Hou, W., S. Hu, Z. Su, et al., Myricetin attenuates LPS-induced inflammation in RAW 264.7 macrophages and mouse models. Future Med Chem, 10 (2018) 2253-2264. https://doi.org/10.4155/fmc-2018-0172.

[29] Wang, L., H. Wu, F. Yang, et al., The Protective Effects of Myricetin against Cardiovascular Disease. J Nutr Sci Vitaminol (Tokyo), 65 (2019) 470-476. https://doi.org/10.3177/jnsv.65.470.

[30] Guo, C., G. Xue, B. Pan, et al., Myricetin Ameliorates Ethanol-Induced Lipid Accumulation in Liver Cells by Reducing Fatty Acid Biosynthesis. Mol Nutr Food Res, 63 (2019) e1801393. https://doi.org/10.1002/mnfr.201801393.

[31] Hassan, S.M., M.M. Khalaf, S.A. Sadek, et al., Protective effects of apigenin and myricetin against cisplatin-induced nephrotoxicity in mice. Pharm Biol, 55 (2017) 766-774. https://doi.org/10.1080/13880209.2016.1275704.

[32] Qi, S., Z. Feng, Q. Li, et al., Myricitrin Modulates NADPH Oxidase-Dependent ROS Production to Inhibit Endotoxin-Mediated Inflammation by Blocking the JAK/STAT1 and NOX2/p47(phox) Pathways. Oxid Med Cell Longev, 2017 (2017) 9738745. https://doi.org/10.1155/2017/9738745.

[33] Qiu, Y., N. Cong, M. Liang, et al., Systems Pharmacology Dissection of the Protective Effect of Myricetin Against Acute Ischemia/Reperfusion-Induced Myocardial Injury in Isolated Rat Heart. Cardiovasc Toxicol, 17 (2017) 277-286. https://doi.org/10.1007/s12012-016-9382-y.

[34] Liao, H.H., N. Zhang, Y.Y. Meng, et al., Myricetin Alleviates Pathological Cardiac Hypertrophy via TRAF6/TAK1/MAPK and Nrf2 Signaling Pathway. Oxid Med Cell Longev, 2019 (2019) 6304058. https://doi.org/10.1155/2019/6304058.

[35] Lv, H., B. An, Q. Yu, et al., The hepatoprotective effect of myricetin against lipopolysaccharide and D-galactosamine-induced fulminant hepatitis. Int J Biol Macromol, 155 (2020) 1092-1104. https://doi.org/10.1016/j.ijbiomac.2019.11.075.

[36] Xia, W., J. Xiao, C. Tong, et al., Orientin inhibits inflammation in chondrocytes and attenuates osteoarthritis through Nrf2/NF-kappaB and SIRT6/NF-kappaB pathway. J Orthop Res, 41 (2023) 2405-2417. https://doi.org/10.1002/jor.25573.

[37] Wang, L., S. Jing, H. Qu, et al., Orientin mediates protection against MRSA-induced pneumonia by inhibiting Sortase A. Virulence, 12 (2021) 2149-2161. https://doi.org/10.1080/21505594.2021.1962138.

[38] Hua, Z., W. Zhang, L. Han, et al., Kaempferol exerts antioxidant effects in age-related diminished ovarian reserve by regulating the HSP90/NRF2 pathway. Chem Biol Drug Des, 103 (2024) e14385. https://doi.org/10.1111/cbdd.14385.

[39] Ji, X., C. Zhang, J. Yang, et al., Kaempferol Improves Exercise Performance by Regulating Glucose Uptake, Mitochondrial Biogenesis, and Protein Synthesis via PI3K/AKT and MAPK Signaling Pathways. Foods, 13 (2024). https://doi.org/10.3390/foods13071068.

[40] Cheng, D., X. Liu, Y. Gao, et al., alpha-Ketoglutarate Attenuates Hyperlipidemia-Induced Endothelial Damage by Activating the Erk-Nrf2 Signaling Pathway to Inhibit Oxidative Stress and Mitochondrial Dysfunction. Antioxid Redox Signal, 39 (2023) 777-793. https://doi.org/10.1089/ars.2022.0215.

[41] Zhang, Z., J. Wu, C. Teng, et al., Orientin downregulating oxidative stress-mediated endoplasmic reticulum stress and mitochondrial dysfunction through AMPK/SIRT1 pathway in rat nucleus pulposus cells in vitro and attenuated intervertebral disc degeneration in vivo. Apoptosis, 27 (2022) 1031-1048. https://doi.org/10.1007/s10495-022-01770-9.

[42] Liu, K., X. Li, Z. Liu, et al., Orientin Promotes Antioxidant Capacity, Mitochondrial Biogenesis, and Fiber Transformation in Skeletal Muscles through the AMPK Pathway. J Agric Food Chem, 72 (2024) 6226-6235. https://doi.org/10.1021/acs.jafc.3c08039.

[43] Nguyen, T., P. Nioi, and C.B. Pickett, The Nrf2-antioxidant response element signaling pathway and its activation by oxidative stress. J Biol Chem, 284 (2009) 13291-5. https://doi.org/10.1074/jbc.R900010200.

[44] Zhang, Q., J. Liu, H. Duan, et al., Activation of Nrf2/HO-1 signaling: An important molecular mechanism of herbal medicine in the treatment of atherosclerosis via the protection of vascular endothelial cells from oxidative stress. J Adv Res, 34 (2021) 43-63. https://doi.org/10.1016/j.jare.2021.06.023.

[45] Ghareghomi, S., F. Moosavi-Movahedi, L. Saso, et al., Modulation of Nrf2/HO-1 by Natural Compounds in Lung Cancer. Antioxidants (Basel), 12 (2023). https://doi.org/10.3390/antiox12030735.

[46] Han, B., S. Li, Y. Lv, et al., Dietary melatonin attenuates chromium-induced lung injury via activating the Sirt1/Pgc-1alpha/Nrf2 pathway. Food Funct, 10 (2019) 5555-5565. https://doi.org/10.1039/c9fo01152h.

[47] Zhang, K., M. Han, X. Zhao, et al., Hypoglycemic and Antioxidant Properties of Extracts and Fractions from Polygoni Avicularis Herba. Molecules, 27 (2022). https://doi.org/10.3390/molecules27113381.

[48] Conde-Hernandez, L.A. and J.A. Guerrero-Beltran, Total phenolics and antioxidant activity of Piper auritum and Porophyllum ruderale. Food Chem, 142 (2014) 455-60. https://doi.org/10.1016/j.foodchem.2013.07.078.

[49] Chen, M., J. Xiao, H.R. El-Seedi, et al., Kaempferol and atherosclerosis: From mechanism to medicine. Crit Rev Food Sci Nutr, 64 (2024) 2157-2175. https://doi.org/10.1080/10408398.2022.2121261.

[50] Hussain, M.S., A.S.A. Altamimi, M. Afzal, et al., Kaempferol: Paving the path for advanced treatments in aging-related diseases. Exp Gerontol, 188 (2024) 112389. https://doi.org/10.1016/j.exger.2024.112389.

[51] Zhu, H., Y. Yan, Y. Jiang, et al., Ellagic Acid and Its Anti-Aging Effects on Central Nervous System. Int J Mol Sci, 23 (2022). https://doi.org/10.3390/ijms231810937.

[52] Lu, G., X. Wang, M. Cheng, et al., The multifaceted mechanisms of ellagic acid in the treatment of tumors: State-of-the-art. Biomed Pharmacother, 165 (2023) 115132. https://doi.org/10.1016/j.biopha.2023.115132.

[53] Li, J., H. Jiang, P. Wu, et al., Toxicological effects of deltamethrin on quail cerebrum: Weakened antioxidant defense and enhanced apoptosis. Environ Pollut, 286 (2021) 117319. https://doi.org/10.1016/j.envpol.2021.117319.

[54] Yang, Q., B. Han, S. Li, et al., The link between deacetylation and hepatotoxicity induced by exposure to hexavalent chromium. J Adv Res, 35 (2022) 129-140. https://doi.org/10.1016/j.jare.2021.04.002.

[55] Hussain, T., B. Tan, Y. Yin, et al., Oxidative Stress and Inflammation: What Polyphenols Can Do for Us? Oxid Med Cell Longev, 2016 (2016) 7432797. https://doi.org/10.1155/2016/7432797.

[56] McGarry, T., M. Biniecka, D.J. Veale, et al., Hypoxia, oxidative stress and inflammation. Free Radic Biol Med, 125 (2018) 15-24. https://doi.org/10.1016/j.freeradbiomed.2018.03.042.

[57] Zhang, Z., L. Zhao, X. Zhou, et al., Role of inflammation, immunity, and oxidative stress in hypertension: New insights and potential therapeutic targets. Front Immunol, 13 (2022) 1098725. https://doi.org/10.3389/fimmu.2022.1098725.

[58] Wei, C., X. Chen, D. Chen, et al., Dihydromyricetin Enhances Intestinal Antioxidant Capacity of Growing-Finishing Pigs by Activating ERK/Nrf2/HO-1 Signaling Pathway. Antioxidants (Basel), 11 (2022). https://doi.org/10.3390/antiox11040704.

[59] Yang, S.Y., M.C. Pyo, M.H. Nam, et al., ERK/Nrf2 pathway activation by caffeic acid in HepG2 cells alleviates its hepatocellular damage caused by t-butylhydroperoxide-induced oxidative stress. BMC Complement Altern Med, 19 (2019) 139. https://doi.org/10.1186/s12906-019-2551-3.